Journal of Theoretical Biology 397 (2016) 52–60

Contents lists available at ScienceDirect

Journal of Theoretical Biology

journal homepage: www.elsevier.com/locate/yjtbi

Mathematical model for calcium-assisted epidermal homeostasis

Yasuaki Kobayashi [a,b,*], Yusuke Sawabu [c], Hiroyuki Kitahata [d], Mitsuhiro Denda [e,b], Masaharu Nagayama [a,b,*]

[a] Research Institute for Electronic Science, Hokkaido University, N12W7, Kita-ku, Sapporo 060-0812, Japan
[b] CREST, Japan Science and Technology Agency, Gobancho, Chiyoda-ku, Tokyo 102-0076, Japan
[c] Department of Mathematics, Graduate School of Science, Hokkaido University, N12W7, Kita-ku, Sapporo 060-0812, Japan
[d] Department of Physics, Graduate School of Science, Chiba University, Yayoi-cho 1-33, Chiba 263-8522, Japan
[e] Shiseido Research Center, Shiseido Co., Ltd., 2-12-1 Fukuura, Kanazawa-ku, Yokohama 236-8643, Japan

HIGHLIGHTS

- A stabilization mechanism of the epidermal structure is proposed.
- The mechanism relies on calcium-induced enhancement of differentiation.
- Key features of epidermal barrier recovery are numerically reproduced.

ARTICLE INFO

Article history:
Received 5 November 2015
Received in revised form
23 February 2016
Accepted 24 February 2016
Available online 4 March 2016

Keywords:
Reaction-diffusion system
Dermatology
Dynamical system

ABSTRACT

Using a mathematical model of the epidermis, we propose a mechanism of epidermal homeostasis mediated by calcium dynamics. We show that calcium dynamics beneath the stratum corneum can reduce spatio-temporal fluctuations of the layered structure of the epidermis. We also demonstrate that our model can reproduce experimental results that the recovery from a barrier disruption is faster when the disrupted site is exposed to air. In particular, simulation results indicate that the recovery speed depends on the size of barrier disruption.

1. Introduction

It is widely recognized that skin is not just a boundary demarcating the body from the environment, but serves as a barrier, particularly against water loss (Elias and Feingold, 2006). Responsible for this barrier function is the *stratum corneum* (SC), the outermost structure of the epidermis, which consists of cornified cells and inter-cellular lipids. In healthy normal skin, its barrier function is fully expressed by ordered arrangement of the cornified cells (Elias and Feingold, 2006), and, therefore, structural disruption caused by skin diseases such as atopic dermatitis and psoriasis can lead to deterioration of the barrier function (Harding, 2004).

Epidermal cells produced in the basal layer start a differentiation process during migration to the upper layers, undergo cornification to become part of the SC, and finally get removed from the surface (desquamation). In this continuous supply and removal of cells, an ordered layer structure of the SC emerges in a self-organized manner as a dissipative structure, in the sense that it can be recovered in a few days when its structure is mechanically disturbed (Elias and Feingold, 2006).

Mathematical modeling is quite often useful to get insights into the underlying mechanism of such self-organized systems, and epidermal models have been proposed so far: Nakaoka and Aihara (2013) proposed a lattice model of stochastic cell dynamics. Also, Schaller and Meyer-Hermann (2007) proposed a particle dynamics model to account for tumor growth. In both models, homeostasis is discussed in terms of the population of cells in individual layers of the epidermis. In order to understand epidermal homeostasis in relation to its barrier function, however, we also need to focus on spatio-temporal structures of the SC. Several particle-based models have been proposed for epidermal structures (Stekel et al.,

* Corresponding authors at: Research Institute for Electronic Science, Hokkaido University, N12W7, Kita-ku, Sapporo 060-0812, Japan.
E-mail addresses: yasuaki.kobayashi@es.hokudai.ac.jp (Y. Kobayashi), nagayama@es.hokudai.ac.jp (M. Nagayama).

http://dx.doi.org/10.1016/j.jtbi.2016.02.032

1995; Rashbass et al., 1996; Maheswaran et al., 2007), although they do not succeed in forming a flat structure of the SC.

Recent studies have revealed that calcium plays important roles on epidermal homeostasis. For instance, genetic skin diseases can be induced by the mutation of the calcium pump and gap junctions (Sakuntabhai et al., 1999; Hu et al., 2000; Mese et al., 2007), and abnormal calcium distribution is observed in diseased skin (Forslind et al., 1999). More precisely, it has been reported that the calcium distribution beneath the SC is closely related to the status of the skin: in normal skin, a localized layer of calcium was observed in the cells just below the SC; and when the SC was impaired, this localization of calcium was lost (Mauro et al., 1998; Denda et al., 2000). Also, calcium wave propagation was found in cultured keratinocytes (grate majority of epidermal cells) when exposed to air (Denda and Denda, 2007), which implies the relationship between calcium signaling and the damage of the skin. These findings seem to make a strong case that calcium localization has an important role in the maintenance and the recovery of the SC.

Although the calcium localization in the epidermis has been mathematically modeled by Cornelissen et al. (2007) and then by Adams et al. (2012), how it affects the structure of the epidermis is still unclear. The effect of calcium ions on proliferation and differentiation has been introduced into a particle-based model (Walker et al., 2006; Sun et al., 2007) to investigate colony formation of keratinocytes, but its effect on the structure of the epidermis has not been addressed. Also, Grabe and Neuber (2005) has simulated the epidermal structure using a particle-based model that takes into account calcium ions, which reproduced a flat epidermal surface. However, the role of calcium ions in the mathematical model is unclear, and hence their model gives little insight into the mechanism for the creation of a flat SC.

In this paper, we propose a particle-based mathematical model of the epidermis where calcium dynamics is incorporated, and demonstrate that epidermal homeostasis can be maintained with the aid of calcium dynamics. In particular, we will show that calcium dynamics can suppress spatio-temporal fluctuation of the boundary of the stratum corneum. Using this model, we will also perform numerical experiments on barrier disruption to investigate a possible role of calcium dynamics on the recovery process.

Epidermal homeostasis is strongly disturbed by various kinds of skin diseases, and the involvement of calcium in such skin disorders is reported (Proksch et al., 2008). Since our calcium model is based on actual responses of the keratinocytes to mechanical stimuli under various conditions (Kobayashi et al., 2014), effects of these factors can in principle be investigated with our model. It is thus expected that our model might be used as a tool for the numerical investigation of skin diseases.

2. The model

We formulate our model of epidermis by taking into account the following properties: reproduction in the basal layer, migration towards the outer layers, differentiation, and calcium dynamics.

Cell i is represented as a sphere with the position $\boldsymbol{x}_i(t)=(x_i(t), y_i(t), z_i(t))$ and the radius $r_i(t)$, defined in a three-dimensional space $\Omega=[0,L_x]\times[0,L_y]\times[0,L_z]$, where the plane $z=0$ defines the boundary of the dermis. On top of the dermis we have the basal layer, defined as $0<z<z^*$, which contains proliferating cells, and on top of it is the suprabasal layer, defined as $z\geq z^*$, where cells are in the process of differentiation or cornified. Proliferation and differentiation are characterized by the phase $\phi_i(t)$ and the state variable $S_i(t)$, respectively. In particular, cornification occurs when the state variable reaches a certain value. Both proliferation and differentiation are affected by the intra-cellular calcium, denoted by $c_i(t)$. Dynamics of each variable is detailed below.

2.1. Cell reproduction in the basal layer

In the basal layer, we assume two types of proliferative cells: stem cells can reproduce infinite number of times, while transit amplifying (TA) cells can reproduce only finite times. A stem cell reproduces one TA cell, and a TA cell reproduces itself.

The phase of the cell division cycle $\phi_i(t)$ evolves in time as

$$\dot{\phi}_i=\omega+\alpha(c_i-c_0)_+, \tag{1}$$

where $(x)_+$ equals x if x is positive and otherwise 0; ω, α, and c_0 are constants; c_0 is the value of calcium at the rest state. It is assumed that the cell cycle accelerates when intra-cellular calcium increases, reflecting an experimental result (Rizk-Rabin and Pavlovitch, 1993; Vandenberghe et al., 2013). When $\phi_i=2\pi$, the cell i enters the cell division period, where the division occurs in a stochastic way, following the Poisson process with the rate γ_{div}. Therefore, in the absence of calcium excitation ($\dot{\phi}_i=\omega$), the average cell division time is given by $T_{\mathrm{div}}=2\pi/\omega+1/\gamma_{\mathrm{div}}$.

When cell i at $\boldsymbol{x}_i$ with the radius r_i exhibits a cell division, two new cells j, k are provided with the radii $r_{j,k}=r_i/2$ and the positions:

$$\boldsymbol{x}_{j,k}=\boldsymbol{x}_i\pm\boldsymbol{t}\frac{r_i}{2}, \tag{2}$$

where the positive and the negative signs correspond to j and k, respectively; the unit vector $\boldsymbol{t}$ is tangent to the dermal surface $z=0$, and its orientation is randomly assigned. After the cell division, the radius grows according to the logistic equation:

$$\dot{r}_j=Cr_j(r_{\max}-r_j). \tag{3}$$

The parameters $\omega, \gamma_{\mathrm{div}}$, and C are chosen in such a way that the cell maximally grows before a next cell division cycle comes. Hence a newly born cell is eventually assigned the initial radius $r_j=r_{\max}/2$. Cells created by a stem cell are assigned the maximum number of cell divisions; cells created by a TA cell with $m>0$ remaining cell divisions are assigned $m-1$ remaining cell divisions; TA cells with $m=0$ do not commit a cell division.

We assume that, while the stem cells are tightly bound to the dermis, TA cells are comparatively loosely bound, so that the TA cells can migrate to the suprabasal layer. Once a TA cell leaves the basal layer, it is considered to start a differentiation process, and the binding force to the dermis is set to zero.

2.2. Differentiation in the suprabasal layer

The differentiation process is determined by the variable $S_i(t)$: $S_i=0$ for cells in the basal layer, and $S_i>0$ for cells in the suprabasal layer. Differentiation process starts when cells leave the basal layer and enter the suprabasal layer, where S_i obeys the following calcium-dependent dynamics:

$$\dot{S}_i=\omega'+\alpha'(c_i-c_0)_+, \tag{4}$$

where ω' and α' are constants: the constant ω' reflects the advance of differentiation in the presence of extra-cellular calcium (Elias et al., 2002). Differentiation is also affected by intra-cellular calcium (Fuchs, 1990; Hennings et al., 1980; Boyce and Ham, 1983). Cells undergo cornification at $S_i=S_{\mathrm{SC}}$, and desquamation at $S_i=S_d$. Thus the cells with $S_{\mathrm{SC}}\leq S_i\leq S_d$ form the SC.

2.3. Kinetic interaction among cells

Cells produced in the basal layer migrate outward by the excluded volume effect: we assume a short-range repulsive

interaction among cells which prevent their overlapping. Their dynamics are described by the following overdamped equation of motion:

$$\mu\dot{\boldsymbol{x}}_i = -\frac{\partial}{\partial \boldsymbol{x}_i}\left(\sum_j V_{\mathrm{LJ}}(|\boldsymbol{x}_i-\boldsymbol{x}_j|; r_i, r_j)+E_i\right). \tag{5}$$

Summation is taken over the cells which are in the vicinity of the cell i defined as $|\boldsymbol{x}_i-\boldsymbol{x}_j| \le d^*(r_i+r_j)$, where the constant d^* is chosen in such a way that the interaction at $|\boldsymbol{x}_i-\boldsymbol{x}_j| = d^*(r_i+r_j)$ is sufficiently small and thus negligible. The potential E_i represents the binding to the dermis. For cells in the suprabasal layer $E_i = 0$; for cells in the basal layer, the following elastic potential is assigned:

$$E_i = \frac{K_{s,t}}{2}(z_i - r_i)^2, \tag{6}$$

where K_s and K_t correspond to the force constants for the stem cell and the TA cell, respectively. We assume $K_s > K_t$, and the values are chosen in such a way that only the TA cells have a chance to leave the basal layer. The elastic force vanishes when the cell leaves the basal layer. We have confirmed that, with a proper choice of parameters, stem cells stayed in the basal layer throughout the numerical simulations.

The potential V_{LJ} must be chosen so as to realize the excluded volume effect. Here we have assumed the Lennard-Jones-type short-range repulsive interaction with weak attraction:

$$V_{\mathrm{LJ}}(r; r_i, r_j) = \epsilon\left\{\left(\frac{r_i+r_j}{r}\right)^6 - \frac{1}{2}\left(\frac{r_i+r_j}{r}\right)^{12}\right\}. \tag{7}$$

2.4. Calcium dynamics model

For the dynamics of $c_i(t)$, we adopt our previous model for in vitro calcium dynamics in keratinocytes (Kobayashi et al., 2014), the basic ideas of which are as follows:

Each keratinocyte stores calcium ions in the endoplasmic reticulum (ER). The ER releases calcium ions when one of the two receptors for calcium ions and another one for inositol trisphosphate (IP_3) are activated, and this fast activation is followed by slow inactivation. IP_3 is synthesized inside the cell when extracellular ATP molecules are detected by ATP receptors on cell membranes. Excitations of neighboring cells are induced by the diffusion of ATP outside the cells and that of IP_3 and calcium ions through gap junctions.

Thus our calcium model consists of $A(x,t)$ (extra-cellular ATP concentration), $P_i(t)$ (IP_3 concentration in the ith cell), $c_i(t)$ (calcium ion concentration in the ith cell), $w_{ij}(t)$ (activity of the gap-junctions between cells i and j), and $h_i(t)$ (inactivation variable of the ith cell). In the previous work (Kobayashi et al., 2014), we successfully described finite-range wave propagation that was found in an experiment of mechanically stimulated cultured keratinocytes by using this model. For the present purpose, we modify the previous model to represent the keratinocytes' dependence on the degree of differentiation, such as the gap-junction conductivity, the timescale of the inactivation variable, and the sensitivity to ATP. The details of the model are described in the Appendix.

Interestingly, our previous model could also reproduce a localized ring pattern around a dead cell, which was also experimentally observed (Tsutsumi et al., 2013). In this experiment, it was suspected that some stimulant released by the dead cell caused the localized ring-like calcium excitation. We speculate that this localized ring pattern is the origin of the formation of calcium localization beneath the SC, where keratinocytes might release some stimulants prior to cornification.

Hence, in addition to the above modification, we assume that a stimulant $B(\boldsymbol{x},t)$, which induces calcium excitation, is released by a cell whose state variable $S_i(t)$ is close to the threshold of cornification, and consider the following dynamics of $B(\boldsymbol{x},t)$:

$$\frac{\partial B(\boldsymbol{x},t)}{\partial t} = d_B\Delta B - \kappa_B B + F_0\sum_j \theta(r_j - |\boldsymbol{x}-\boldsymbol{x}_j|)\theta(S_j(t)-S_1)\theta(S_2-S_j(t)), \tag{8}$$

where $\theta(x)$ is the Heaviside function, and the constants S_1 and S_2 are chosen so as to satisfy $S_1 < S_{\mathrm{SC}} < S_2$. The summation is taken over the suprabasal cells.

Cornified cells are considered to be dead, and thus they do not participate in calcium dynamics: their calcium levels are set to c_0.

2.5. Numerical simulation

For numerical simulation, we set the time step $\Delta t = 0.01$. The system size is $(L_x, L_y, L_z) = (50.0, 50.0, 100.0)$. For particle dynamics, periodic boundary conditions are applied in x and y. We have confirmed in numerical simulations that L_z is sufficiently large so that the uppermost particles are removed by desquamation before reaching $z = L_z$.

The parameters for calcium dynamics are given according to our previous work (Kobayashi et al., 2014), where the values are chosen in such a way that basic features of calcium dynamics are reproduced (also see the Appendix). The other parameters are determined in such a way that the numerical results approximate real epidermis as good as possible. In particular, the following data are used for the guidance: the average turnover period ($\sim$28 days), the period from the start of differentiation to terminal differentiation ($\sim$14 days), the cell division period ($\sim$2 days), the average thickness of the epidermis ($\sim$50 μm), and the typical cell size ($\sim$5 μm). With the time scales being measured by the cell division period, we obtain two non-dimensionalized parameters, namely the renormalized turnover period $\tau_t = 14$ and the renormalized differentiation period $\tau_d = 7$. Similarly, the thickness of the epidermis is rescaled by the cell size to obtain the renormalized thickness $h = 10$. Also, the strength of the source of the stimulant, which affects the thickness of the calcium localization layer, is determined so as to ensure that this thickness is limited to one cell layer. The corresponding parameter values are chosen as follows: $\omega = 0.0170, \alpha = 0.698, c_0 = 0.122, \gamma_{\mathrm{div}} = 0.00813, z^* = 2.4, r_{\max} = 1.4, \omega' = 0.005, \alpha' = 0.05, S_{\mathrm{SC}} = 22.0, S_d = 31.3, \mu = 1.0, d^* = 1.3, K_s = 5.0, K_t = 0.5, \epsilon = 1.0, S_1 = 21.4, S_2 = 22.5, d_B = 0.0009, \kappa_B = 0.025$, and $F_0 = 1.0$.

In the basal layer, eight stem cells are randomly placed, which approximately account for four percent of the total population in this layer. The maximum number of cell divisions of the TA cells are set to ten.

The timescale of calcium dynamics in the epidermis is the order of seconds and minutes. On the other hand, cell division and the accompanying migration are of the order of hours. Therefore it is expected that different timescale can be utilized to calculate calcium dynamics. Since major change of calcium distribution in our system occurs when a cell cornifies, where the stimulant secreted from the cornified cell excites the neighboring cells, we adopt the following computation algorithm. We calculate the cell dynamics [Eqs. (1), (3), (4), and (5)] together with the dynamics of the stimulant (8) with the calcium levels kept as constant. When a certain number of cells (we choose 20 throughout our simulations) cornify, we switch to the computation of calcium dynamics [Eqs. (19)–(23)] for a certain time interval, with the variables $(\boldsymbol{r}_i, S_i, \phi_i, B)$ unchanged, until the system reaches a steady state. Then we return to the cell dynamics, where the obtained equilibrium calcium levels are assigned.

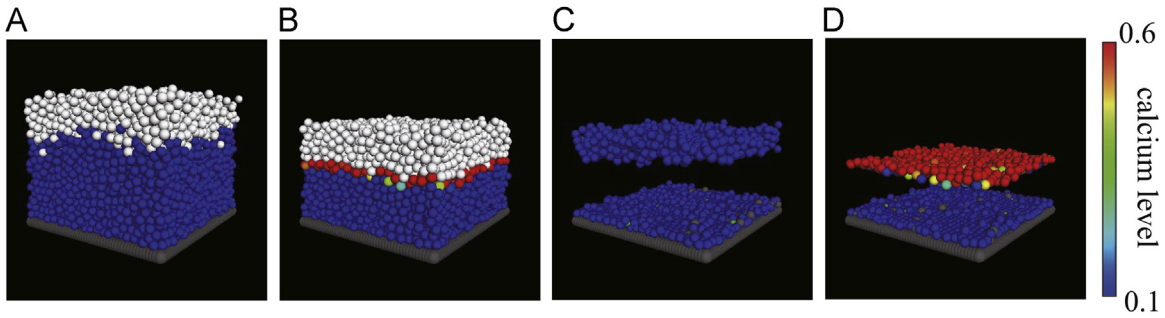

Fig. 1. Numerical simulation of the epidermis with and without calcium dynamics. (A,B) whole structure of the calculated epidermis, without calcium dynamics (A) and with calcium dynamics (B). The dermal boundary at the bottom is colored gray; cornified cells are represented by white spheres; non-cornified cells are colored depending on the calcium level. (C,D) Visualization of only the basal layer and the boundary layer; (C) and (D) correspond to (A) and (B), respectively. The basal layer contains stem cells (green) and TA cells which are reproducible (blue) or no longer reproducible (gray). (For interpretation of the references to color in this figure caption, the reader is referred to the web version of this paper.)

3. Numerical results

3.1. Calcium suppresses spatio-temporal fluctuations

Here we ask if a well-defined cornified cell layer emerges as a steady state. To see how calcium dynamics affects the overall behavior of the model epidermis, we first perform a numerical simulation with computing calcium dynamics, fixing all values of $c_i(t)$ to $c_i(t)=c_0$. The result is shown in Fig. 1(A), where cornified cells are intermingled with non-cornified cells, and their boundary is unclear. In contrast, when we compute a full model, including calcium dynamics, the boundary becomes clearer, as shown in Fig. 1(B). The difference is more visible if we compare Fig. 1(C) (without calcium dynamics) and Fig. 1(D) (with calcium dynamics), where, in addition to the basal layer, we show the *boundary layer*, a set of non-cornified suprabasal cells which are in contact with the cornified cells. Here the spatial homogeneity of the SC boundary is more obvious. It is also noted that, in Fig. 1(D), the cells in the boundary layer exhibit calcium excitation. In other words, a calcium localization layer is formed beneath the stratum corneum.

In our model, calcium affects both the speed of terminal differentiation and the cell division (Eqs. (4) and (1)). In order to check the effect of calcium more precisely, we introduce a parameter λ, the modifier of calcium dynamics, and replace the parameters α and α' in Eqs. (4) and (1) with $\lambda\alpha$ and $\lambda\alpha'$. For different values of λ we measure the number of TA cells $[n_{\mathrm{ta}}(t)]$, the suprabasal cells which are non-cornified $[n_{\mathrm{nc}}(t)]$ or cornified $[n_{\mathrm{c}}(t)]$, and the cells in the boundary layer $[n_{\mathrm{b}}(t)]$. Fig. 2 shows the time average of these values, denoted by $\langle\cdots\rangle$, against λ. Error bars represent the standard deviation obtained from the temporal variation. We observe that, while $\langle n_{\mathrm{ta}}\rangle$ and $\langle n_{\mathrm{c}}\rangle$ remains unchanged, $\langle n_{\mathrm{nc}}\rangle$ and $\langle n_{\mathrm{b}}\rangle$ decreases as λ increases. In particular, $\langle n_{\mathrm{b}}\rangle$ decreases faster than $\langle n_{\mathrm{nc}}\rangle$. The standard deviation of $n_{\mathrm{b}}(t)$ also decrease, while those of the other three show no significant differences, being small regardless of the values of λ. In other words, populations in the three regions are well maintained even when we neglect calcium dynamics, while the boundary is strongly affected by calcium dynamics.

These observations can be understood as follows: constant values of $\langle n_{\mathrm{ta}}\rangle$ and $\langle n_{\mathrm{c}}\rangle$ with respect to λ reflect the fact that calcium is well localized around the boundary layer and does not affect the basal layer nor the SC; the linear dependence of $\langle n_{\mathrm{nc}}\rangle$ reflects the fact that the thickness of the entire epidermis decreases linearly with λ, presumably caused by calcium-aided acceleration of differentiation; the faster decrease of $\langle n_{\mathrm{b}}\rangle$ reflects the spatial smoothing of the boundary layer, also caused by calcium dynamics. To quantify the degree of spatial homogeneity, we introduce the following cost function:

$$E=\frac{1}{N_b}\sum_{j\in\Omega_b}\frac{(z_j-\bar{z})^2}{r_{\max}^2}, \tag{9}$$

where Ω_b is the set of cells in the boundary layer, N_b is the number of the cells in Ω_b, and $\bar{z}\equiv\sum_{j\in\Omega_b}z_j/N_b$. $E\geq 0$ in general, and $E=0$ when the boundary layer is completely flat. As shown in Fig. 3(A), if calcium dynamics is absent ($\lambda=0$), the cost function E has large values and fluctuates in time, and as λ increases, E tends to have smaller values, with smaller fluctuations. The systematic decrease of the time average $\langle E\rangle$ and the standard deviation (shown as error bars) of $E(t)$ with respect to time are shown in Fig. 3(B). Thus we conclude that, in our model, calcium dynamics suppresses spatial and temporal fluctuations of the boundary layer, contributing to a well-defined layered structure.

Another measure, which quantifies the overlap of the distributions of the non-cornified and cornified suprabasal cells in the z-direction, will illuminate how calcium enhances the layered structure. Let us divide the region $0\leq z\leq L_z$ into N regions, and count the number of the non-cornified suprabasal cells in the m-th region, denoted by P_m^{nc}:

$$P_m^{\mathrm{nc}}=\sum_{j\in\Omega_{\mathrm{nc}}}\chi_m(z_j;\Delta), \tag{10}$$

where Ω_{nc} is the set of non-cornified suprabasal cells, and

$$\chi_m(z;\Delta)=\begin{cases}1 & (m-1)\Delta\leq z<m\Delta,\\ 0 & \text{else},\end{cases} \tag{11}$$

with $\Delta=L_z/N$. The number of the cornified cells in the m th layer, P_m^{c}, can also be defined in the same way as

$$P_m^{\mathrm{c}}=\sum_{j\in\Omega_{\mathrm{c}}}\chi_m(z_j;\Delta), \tag{12}$$

where Ω_{c} is the set of the cornified cells. Then we define the

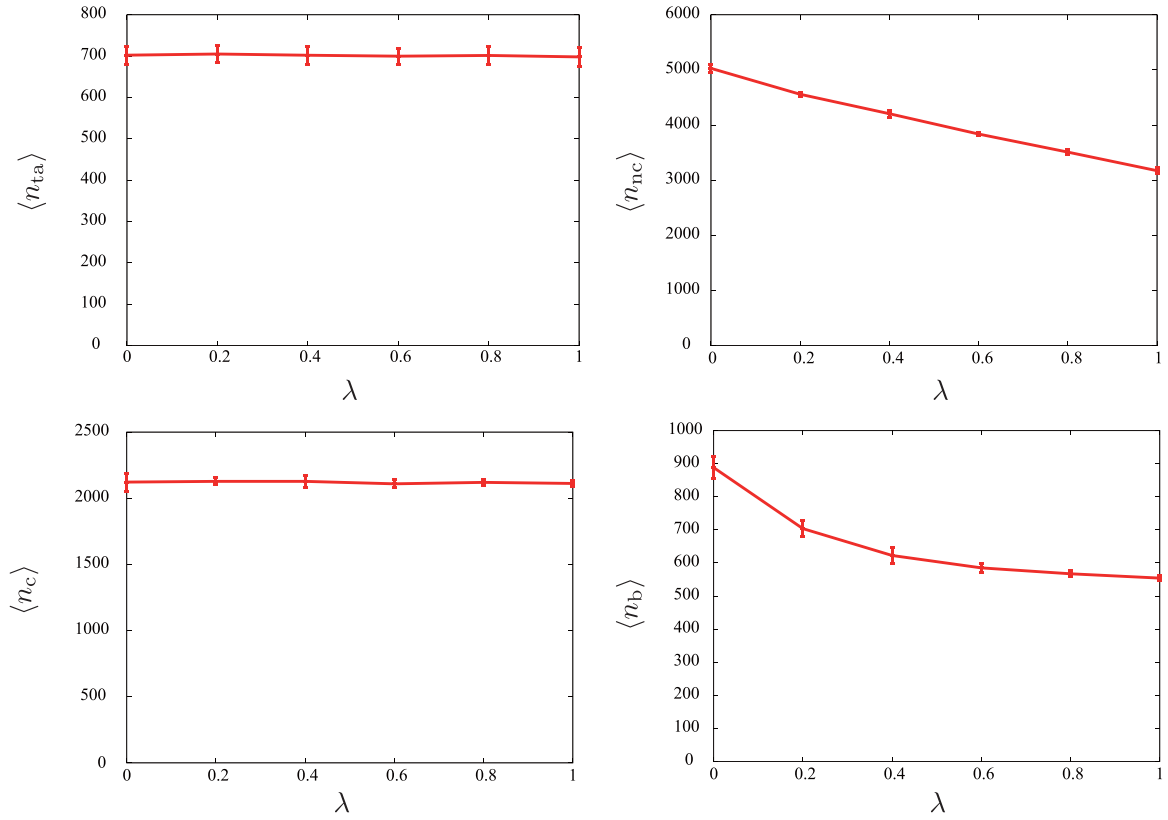

Fig. 2. Calcium dependence of population in individual layers. Time averages of the number of TA cells ($\langle n_{\rm ta} \rangle$), suprabasal cells which are not cornified ($\langle n_{\rm nc} \rangle$), cornified ($\langle n_{\rm c} \rangle$), and cells in the boundary layer ($\langle n_{\rm b} \rangle$), as a function of the modifier of calcium dynamics λ. Error bars represent the standard deviation obtained from the time series.

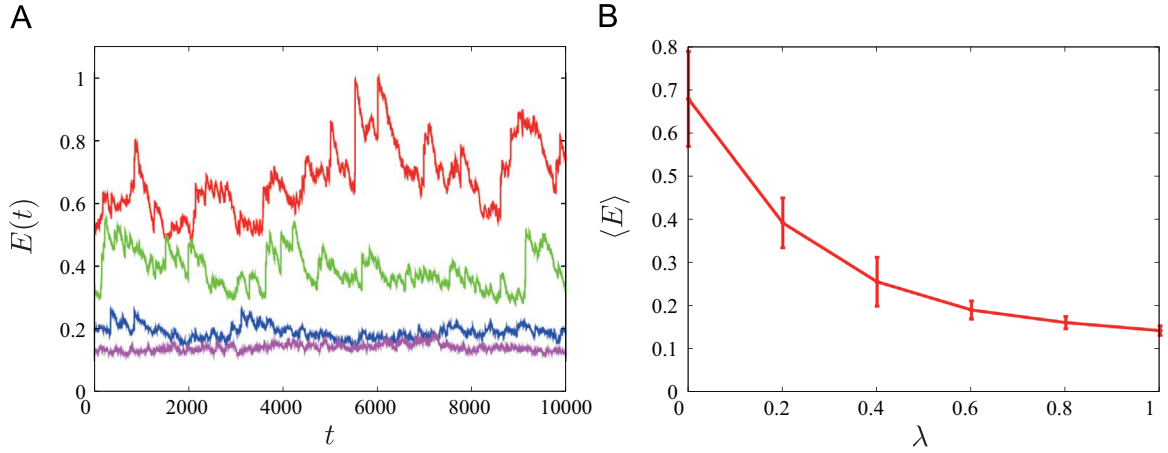

Fig. 3. Calcium dependence of the cost function. (A) Time series of the cost function $E(t)$ for four values of λ : $\lambda = 0.0, 0.2, 0.6$, and 1.0 from top to bottom. (B) Time average of the energy function, $\langle E \rangle$, as a function of λ.

overlap function $I(z)$:

$$I(z) = \sum_{m=1}^{N} \sqrt{P_m^{\rm nc} P_m^{\rm c}} \chi_m(z;\Delta) = \sum_{m=1}^{N} \sqrt{\sum_{j \in \Omega_{\rm nc}} \sum_{k \in \Omega_{\rm c}} \chi_m(z_j;\Delta)\chi_m(z_k;\Delta)}\, \chi_m(z;\Delta). \tag{13}$$

We choose $\Delta = 0.2$. As shown in Fig. 4, $I(z)$ well captures the change of $\langle n_{\rm b} \rangle$ and $\langle n_{\rm nc} \rangle$: As λ decreases, both the width and the peak position of $I(z)$ decrease, which indicates the suppression of the overlapping and the entire thickness.

These results show that the calcium localization layer helps stabilize the shape of the boundary layer, which is consistent with the analysis of a reaction–advection–diffusion model of the epidermis (Kobayashi et al., 2015). In our model, it is assumed that calcium accelerates the cornification process, and cornification in turn induces calcium excitation. Such a relationship between calcium and differentiation might account for some aspects of epidermal homeostasis.

3.2. Recovery from the disruption of the stratum corneum

Next we check if our model can reproduce an important property of the epidermis: recovery from barrier disruption. Grubauer et al. (1989) measured the barrier function of the epidermis after removing part of the SC, and found that the recovery of the barrier slowed down when the disrupted site is not exposed to air. Although the detailed mechanism of this phenomenon is

still unknown, it is experimentally shown (Denda and Denda, 2007) that the ATP concentration is increased when keratinocytes are exposed to air, which then induces calcium excitation. Therefore, we incorporate the effect of air-exposure into our model as follows. We introduce new particles that play a role of air, with the radius $r = r_{\max}$. These particles follow the same kinetic interactions with the suprabasal cells, and when non-cornified cells are in contact with these air particles, they receive air-stimulation, which is realized by the increase of the ATP (see the Appendix).

In numerical simulations of barrier disruption, first we prepare an epidermis in a steady state, which is obtained in the previous calculations, as an initial state. Then at $t = 0$ we remove the SC cells and continue the simulation. In the case of air exposure, we fill the space of the removed cells with air particles. Fig. 5 shows snapshots of the numerical barrier disruption experiment, with and without air exposure. In both cases, recovery of the SC is observed. In the case of air exposure (Fig. 5(A)), we observe a wide range of calcium distribution toward the basal layer. Compared to the case of no air-exposure (Fig. 5(B)), faster reformation of the SC is observed.

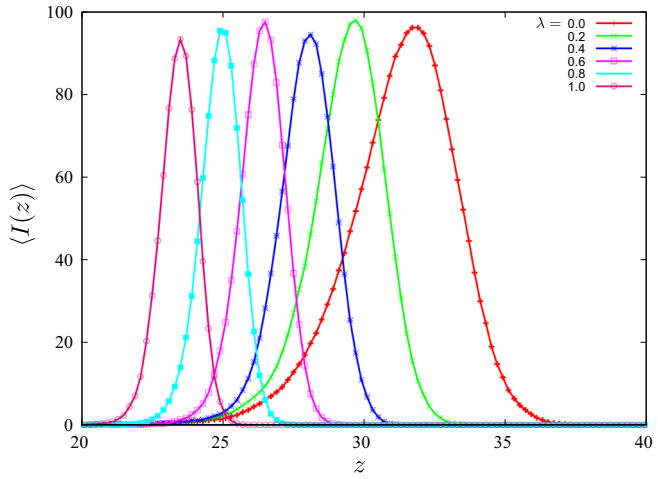

Fig. 4. Calcium dependence of the overlap function. Time average of the overlap function, $\langle I(z)\rangle$, is calculated for six different values of λ: $\lambda = 0.0, 0.2, 0.4, 0.6, 0.8$, and 1.0 from right to left.

In the barrier disruption experiment (Grubauer et al., 1989), barrier function was evaluated in terms of trans-epidermal water loss. For the evaluation of barrier function in numerical simulations, we take an indirect way. Since a relationship is known between lipid secretion and barrier disruption (Menon et al., 1992), we consider the quantity of lipids contained in the SC as a measure of barrier. Hence we introduce a new variable representing lipid quantity, the dynamics of which are dependent on calcium and the state variable.

Dynamics of the lipid quantity are determined as follows: it is well known that lipid synthesis occurs in the granular layer, located beneath the SC (Landmann, 1998). Also, experiments suggest that lipids are synthesized and secreted depending on the calcium level of the cells (Sando et al., 1996; Denda et al., 2003). Hence we introduce two variables, the synthesized lipid quantity $v_i^{\mathrm{syn}}(t)$ and the secreted lipid quantity $v_i^{\mathrm{sec}}(t)$ for cell i, the dynamics of which are determined as a function of c_i and S_i:

$$\frac{dv_i^{\mathrm{syn}}}{dt} = (v_{\max} - v_i^{\mathrm{syn}}) f_{\mathrm{syn}}(c_i, S_i) - f_{\mathrm{sec}}(c_i, S_i), \tag{14}$$

$$\frac{dv_i^{\mathrm{sec}}}{dt} = f_{\mathrm{sec}}(c_i, S_i), \tag{15}$$

where $f_{\mathrm{syn}}(c_i, S_i) = F_1\theta(c^* - c_i)\theta(S - S_{\mathrm{SG}})$, $f_{\mathrm{sec}}(c_i, S_i) = F_2\theta(c_i - c^*)\theta(S_i - S_{\mathrm{SG}})$ and θ is the Heaviside function. Thus the lipid dynamics start at $S_i = S_{\mathrm{SG}} < S_{\mathrm{SC}}$. Lipid is synthesized when the calcium level is low, and secreted when the calcium level is high (Sando et al., 1996; Denda et al., 2003), with the threshold given by c^*.

Eqs. (14) and (15) are solved together with the epidermal dynamics (Eqs. (1), (3)–(5), and (8)) . At each moment, barrier function is determined using calculated v_i^{syn} as follows. Let us divide the region $0 \le x \le L_x$ and $0 \le y \le L_y$ into $M_1 \times M_2$ subregions $(m-1)\Delta_x \le x < m\Delta_x$ and $(n-1)\Delta_y \le y < n\Delta_y$ $(m, n = 1, \ldots, M_{1,2})$, where $\Delta_{x,y} \equiv L_{x,y}/M_{1,2}$, and measure the lipid quantity in the SC at subregion (m, n):

$$\rho_{mn} = \sum_{j \in \Omega_c} \chi_m(x_j; \Delta_x)\chi_n(y_j; \Delta_y)v_j. \tag{16}$$

Then for each subregion we define the penalty function:

$$L_{mn}^{\mathrm{local}} = \begin{cases} 1 - \dfrac{\rho_{mn}}{\rho^*}, & \rho_{mn} < \rho^* \\ 0 & \rho_{mn} \ge \rho^*, \end{cases} \tag{17}$$

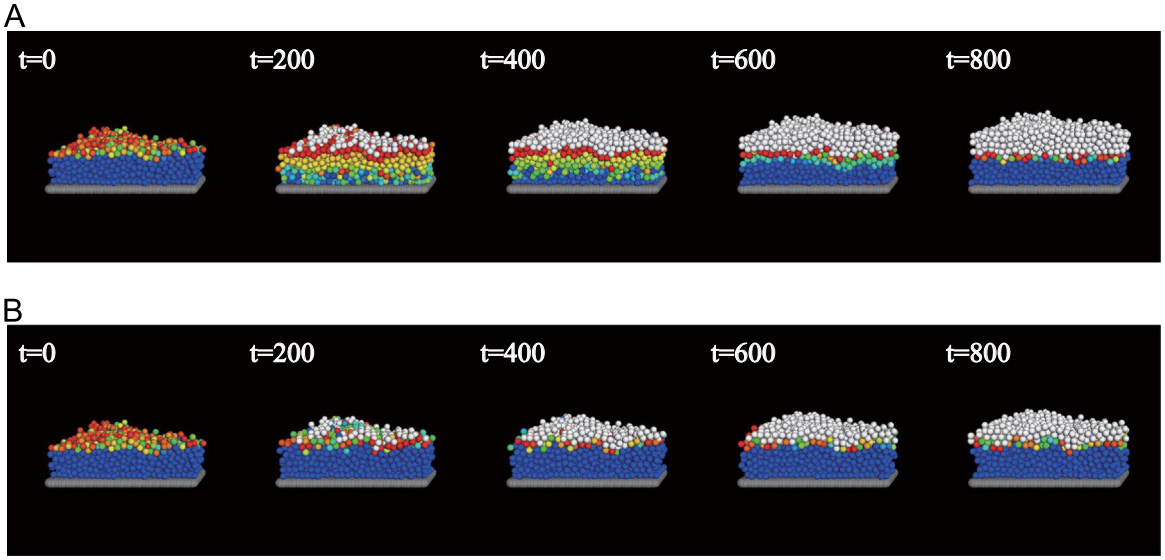

Fig. 5. Numerical simulation of barrier disruption with and without air exposure. (A) Snapshots with air exposure; (B) without air exposure. At $t = 0$, all existing cornified cells are removed from the steady-state epidermis.

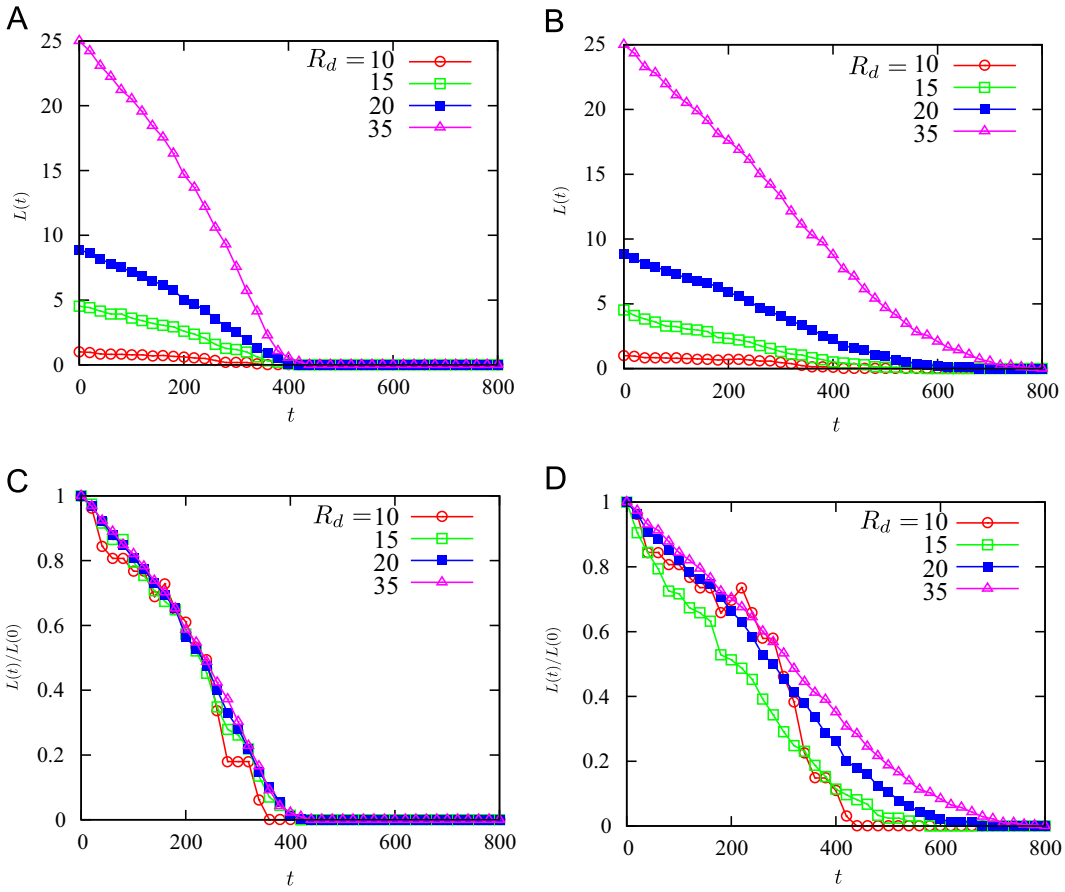

Fig. 6. Recovery of barrier after disruption with and without air exposure. (A,B) Penalty function $L(t)$ as a function of time, with the disruption size $R_d = 5$, 10, 15, and 35: (A) with air-exposure; (B) without air-exposure. (C,D) same plots, rescaled by the initial value $L(0)$: (C) with air-exposure; (D) without air-exposure.

where ρ^* is a constant corresponding to a typical density of lipid for healthy skin. Here we set $\rho^* = \frac{2\Delta_x\Delta_y}{4r_{\max}^2}v_{\max}$, which is equivalent to the assumption that approximately two layers of lipid-loaded cells are sufficient to fully express the barrier function. The penalty function of the entire epidermis is then defined as

$$L = \sum_{m=1}^{M_1}\sum_{n=1}^{M_2} L_{mn}^{\text{local}}. \tag{18}$$

The parameters are chosen as follows: $F_1 = 0.032, F_2 = 0.050$, $c^* = 0.25, S_{SG} = 7.0$, $v_{\max} = 1.0$, and $\Delta_x = \Delta_y = 10.0$.

Using this penalty function as a measure of the barrier function, we performed simulations for barrier disruption for different disruption sizes: we prepare the same steady state epidermis as an initial state as before, and the SC cells in the region $\{(x,y)|x^2+y^2 < R_d^2\}$ are removed, where R_d are chosen to be $R_d = 10, 15, 20$, and 35, the last case corresponding to the removal of all initially existing SC cells. Fig. 6 shows how the barrier function recovers in time with and without air exposure, for different disruption sizes. Fig. 6(A) and (B) shows the penalty function $L(t)$ with and without air exposure, respectively. Obviously the time when $L(t)$ reaches zero becomes longer for Fig. 6(B). To be more precise, while in the case of air-exposure the recovery time seems to converge to a certain value as increasing the disruption size R_d, in the case of no air-exposure the recovery time increases as R_d. This behavior is more visible when the penalty function $L(t)$ is rescaled by the initial value $L(0)$ for individual values of R_d (Fig. 6 (C) and (D)). This size dependence can in principle be tested experimentally.

4. Discussions and summary

The numerical results presented in this paper suggest a possible mechanism for the suppression of spatio-temporal fluctuations in the SC by the formation of the calcium localization layer beneath the SC. It should be emphasized that, even if calcium dynamics are not considered, our model still shows homeostatic properties in terms of population balance in each layer. However, there must be stabilization mechanism due to calcium dynamics to realize spatio-temporal stability of the SC.

We have set aside several important aspects on the epidermis such as shape change of the epidermal cells during differentiation and undulations of the dermis, which must have influence on the homeostasis of the epidermis. Also, adhesion among the cells, which depends on the differentiation process, must affect cell kinetics. Cell elasticity change during differentiation might be another important problem, which can be implemented into our model by assigning to the interaction coefficient ϵ the dependence on the differentiation stage. It is important to investigate to what extent our results are affected by incorporating these aspects.

In the simulation of barrier disruption, we have introduced lipids only for the purpose of monitoring and estimating the barrier function; there is no feedback from lipid dynamics to the other dynamics. As a consequence, the epidermal dynamics is also independent of the status of the barrier function. In reality, the epidermis shows responses to the barrier status (Denda et al., 1998; Wood et al., 1992), and incorporating a feedback loop by considering lipid dynamics-dependence might help enhance the homeostasis. However, it should be noted that, even in our model, a homeostasis property is expressed when the epidermis recovers from disruption, which is enhanced by calcium dynamics.

To summarize, we have developed a mathematical model of epidermal homeostasis, where calcium dynamics is responsible for the stability of the layered structure of the epidermis. Since our calcium model has sufficient details corresponding to experimental results on the behavior of keratinocytes, we expect that our model can also be extended to the study of skin diseases caused by deficiencies in calcium dynamics.

Acknowledgment

The authors acknowledge Prof. Satoshi Nakata (Hiroshima University, Japan) for valuable comments.

Appendix. The model of calcium dynamics

To describe the behavior of calcium, we adopt the model of epidermal calcium propagation in Kobayashi et al. (2014), which is modified here so as to incorporate dependence of the dynamics on the differentiation process, and the effect of air-stimulation in the case of air-exposure simulations. In this model, $c_i(t)$, calcium concentration for cell i, is a function of $P_i(t)$ (concentration of IP_3 in cell i), $h_i(t)$ (inactivation factor), $w_{ij}(t)$ (activity of the gap-junctions between cells i and j, and $A(\boldsymbol{x},t)$) (extracellular ATP concentration), which obey the following equations:

$$\frac{\partial A}{\partial t} = d_A \Delta A - K_{aa} A + \sum_{j=1}^{N} G_1\left(\boldsymbol{x}, \boldsymbol{x}_j, \frac{dc_j}{dt}\right) + \sum_{j \in \Omega_A} G_2(\boldsymbol{x}, \boldsymbol{x}_j), \tag{19}$$

$$\frac{dc_i}{dt} = \sum_{j \in \Lambda_i} d_c w_{ij} I_n(S_i)(c_j - c_i) + F_c(P_i, c_i, h_i) + I_c^{(i)}(B), \tag{20}$$

$$\frac{dP_i}{dt} = \sum_{j \in \Lambda_i} d_P w_{ij} I_n(S_i)(P_j - P_i) + F_P(A, S_i) - K_{pp} P_i, \tag{21}$$

$$\frac{dh_i}{dt} = \frac{1}{\tau_h(S_i)} F_h(c_i, h_i), \tag{22}$$

$$\frac{dw_{ij}}{dt} = \frac{1}{\tau_w} F_w(w_{ij}, c_i, c_j), \tag{23}$$

where

$$G_1\left(\boldsymbol{x}, \boldsymbol{x}_j, \frac{dc_j}{dt}\right) = \theta(r_j - |\boldsymbol{x} - \boldsymbol{x}_j|) K_{ac} R\left(\frac{dc_j}{dt}\right),$$

$$G_2(\boldsymbol{x}, \boldsymbol{x}_j) = \theta(r_j - |\boldsymbol{x} - \boldsymbol{x}_j|) K_{\mathrm{stim}},$$

$$I_n(S_i) = \frac{1}{2}\left(1 + \tanh\left(\frac{S_i - S_{\mathrm{SG}}}{\delta_I}\right)\right),$$

$$F_c(P, c, h) = K_F\left(\mu_0 + \frac{\mu_1 P}{K_\mu + P}\right)\left(\alpha_0 + \frac{(1-\alpha_0)c}{K_1 + c}\right)h - \frac{\gamma c}{K_\gamma + c} + \beta,$$

$$I_c^{(i)}(B) = \begin{cases} \dfrac{K_{bc} B^2}{H_b^2 + B^2} & i \in \Lambda, \\ 0 & i \notin \Lambda. \end{cases}$$

$$F_P(A, S_i) = K(S_i)\frac{A}{H_0 + A}, \quad F_h(c, h) = \frac{K_2^2}{K_2^2 + c^2} - h,$$

$$F_w(w_{ij}, c_i, c_j) = -w_{ij} + \frac{1}{2}\left\{1 + \tanh\left(\frac{w_d - |c_i - c_j|}{\epsilon_w}\right)\right\},$$

$$R(x) = \begin{cases} x & x \geq 0, \\ 0 & x < 0, \end{cases}$$

$$K(S_i) = K_{pa0} + \frac{K_{pa} - K_{pa0}}{2}\tanh\left(\frac{S_{\mathrm{SG}} - S_i}{\delta_K}\right),$$

$$\tau_h(S_i) = \tau_g + \frac{\tau_s - \tau_g}{2}\left(1 + \tanh\left(\frac{S_{\mathrm{SG}} - S_i}{\delta_\tau}\right)\right).$$

Here Λ_i is the set of cells whose element j satisfies $|\boldsymbol{x}_i - \boldsymbol{x}_j| < d^*(r_i + r_j)$, and S_i is the state variable of cell i. The stimulant B remains constant in time during the calculation of calcium dynamics. This formulation differs from the previous work (Kobayashi et al., 2014) in that some parts are state-variable dependent: The state variables affect the gap-junction conductivity (Tsutsumi et al., 2009), the timescale of the inactivation factor (Tsutsumi et al., 2009), and the sensitivity to ATP (Tsutsumi et al., 2009), each corresponding to the functions $I_n(S_i)$, $\tau_h(S_i)$ and $K(S_i)$. Also, the function G_2 represents the ATP release induced by air stimulation (Denda and Denda, 2007), and Ω_A is the set of air particles introduced in Section 3.2. Parameters are chosen as follows: $d_A = 1.0, K_{aa} = 0.5, K_{ac} = 0.002, K_{\mathrm{stim}} = 0.1,\ d_c = 0.01, \delta_I = 1.5,\ K_F = 8.1,\ \mu_0 = 0.567,\ \mu_1 = 1.0, K_\mu = 0.05, \alpha_0 = 0.11, K_1 = 0.7,\ \gamma = 2.0, K_\gamma = 0.1,\ \beta = 0.02, K_{bc} = 0.4, H_b = 0.1, d_P = 0.1, K_{pa0} = 6.0, K_{pa} = 4.0, H_0 = 0.5,\ \delta_K = 1.0, K_{pp} = 0.3, \tau_s = 1.0, \tau_g = 0.2, \delta_\tau = 1.0, K_2 = 0.7,\ \tau_\omega = 1.0, w_d = 0.1$, and $\epsilon_w = 0.1$.

To solve Eqs. (19) and (8), periodic boundary conditions are assigned in xy directions. The Neumann boundary condition is assigned at $z = 0$. As for the upper boundary, we adopt the following rule: the diffusion constants d_A and d_B at point $\boldsymbol{x}$ are set to zero if the distance to the nearest non-cornified suprabasal particle i, $|\boldsymbol{x} - \boldsymbol{x}_i|$, is greater than a certain threshold l^*, so that chemicals are contained inside the non-cornified suprabasal layer. We choose $l^* = 2r_{\max}$.

References

Adams, M.P., Mallet, D.G., Pettet, G.J., 2012. Active regulation of the epidermal calcium profile. J. Theor. Biol. 301, 112–121.

Boyce, S.T., Ham, R.G., 1983. Calcium-regulated differentiation of normal human epidermal keratinocytes in chemically defined clonal culture and serum-free serial culture. J. Invest. Dermatol. 81, 33–40.

Cornelissen, L.H., Oomens, C.W.J., Huyghe, J.M., Baaijenset, F.P.T., 2007. Mechanisms that play a role in the maintenance of the calcium gradient in the epidermis. Skin Res. Technol. 13, 369–376.

Denda, M., Denda, S., 2007. Air-exposed keratinocytes exhibited intracellular oscillation. Skin Res. Technol. 13, 195–201.

Denda, M., Sato, J., Tsuchiya, T., Elias, P.M., Feingold, K.R., 1998. Low humidity stimulates epidermal DNA synthesis and amplifies the yyperproliferative response to barrier disruption: implication for seasonal exacerbations of inflammatory Dermatoses. J. Invest. Dermatol. 111, 873–878.

Denda, M., Hosoi, J., Asida, Y., 2000. Visual imaging of ion distribution in human epidermis. Biochem. Biophys. Res. Commun. 272, 134–137.

Denda, M., Fuziwara, S., Inoue, K., 2003. Influx of calcium and chloride ions into epidermal keratinocytes regulates exocytosis of epidermal lamellar bodies and skin permeability barrier homeostasis. J. Invest. Dermatol. 121, 362–367.

Elias, P.M., Feingold, K.R., 2006. Stratum corneum barrier function: definitions and broad concepts. In: Elias, P.M., Feingold, K.R. (Eds.), Skin Barrier. Taylor& Francis, New York, pp. 1–4.

Elias, P.M., Ahn, S.K., Denda, M., Brown, B.E., Crumrine, D., et al., 2002. Modulations in epidermal calcium regulate the expression of differentiation-specific markers. J. Invest. Dermatol. 119, 1128–1136.

Forslind, B., Werner-Linde, Y., Lindberg, M., Pallon, J., 1999. Elemental analysis mirrors epidermal differentiation. Acta Derm. Venereol. (Stockh.) 79, 12–17.

Fuchs, E., 1990. Epidermal differentiation: the bare essentials. J. Cell. Biol. 111, 2807–2814.

Grabe, N., Neuber, K., 2005. A multicellular systems biology model predicts epidermal morphology, kinetics and Ca^{2+} flow. Bioinformatics 21, 3541–3547.

Grubauer, G., Elias, P.M., Feingold, K.R., 1989. Transepidermal water loss: the signal for recovery of barrier structure and function. J. Lipid Res. 30, 323–333.

Harding, C.R., 2004. The stratum corneum: structure and function in health and disease. Dermatol. Ther. 17, 6–15.

Hennings, H., Michael, D., Cheng, C., Steinert, P., Holbrook, K., et al., 1980. Calcium regulation of growth and differentiation of mouse epidermal cells in culture. Cell 19, 245–254.

Hu, Z., Bonifas, J.M., Beech, J., Bench, G., Shigihara, T., et al., 2000. Mutations in ATP_2C_1, encoding a calcium pump, cause Hailey–Hailey disease. Nat. Genet. 24, 61–65.

Kobayashi, Y., Sanno, Y., Sakai, A., Sawabu, Y., Tsutsumi, M., et al., 2014. Mathematical modeling of calcium waves induced by mechnical stimulation in keratinocytes. PLOS ONE 9 (3), e92650.

Kobayashi, Y., Kitahata, H., Nagayama, M., 2015. Model for calcium-assisted reduction of structural fluctuations in epidermis. Phys. Rev. E 92, 022709-1–022709-7.

Landmann, L., 1998. The epidermal permeability barrier. Anat. Embryol. (Berl). 178, 1–13.
Maheswaran, S., Speight, P.M., Hammond, P., 2007. Modeling epithelial cell behavior and organization. IEEE Trans. Nanobiosci. 6, 77–85.
Mauro, T., Bench, G., Sidderas-Haddad, E., Feingold, K.R., Elias, P.M., et al., 1998. Acute barrier perturbation abolishes the Ca^{2+} and K^{+} gradients in murine epidermis: quantitative measurement using PIXE. J. Invest. Dermatol. 111, 1198–1201.
Menon, G.K., Feingold, K.R., Elias, P.M., 1992. Lamellar body secretory response to barrier disruption. J. Invest. Dermatol. 98, 279–289.
Meşe, G., Richard, G., White, T.W., 2007. Gap junctions: basic structure and function. J. Invest. Dermatol. 127, 2516–2524.
Nakaoka, S., Aihara, K., 2013. Stochastic simulation of structured skin cell population dynamics. J. Math. Biol. 66, 807–835.
Proksch, E., Brandner, J.M., Jensen, J.M., 2008. The skin: an indispensable barrier. Exp. Dermatol. 17, 1063–1072.
Rashbass, J., Stekel, D., Williams, E., 1996. The use of a computer model to simulate epithelial pathologies. J. Pathol. 179, 333–339.
Rizk-Rabin, M., Pavlovitch, J.H., 1993. Epidermal calcium-binding protein: a marker of early differentiation of basal layer keratinocytes of rats. Cell Tissue Res. 272, 161–168.
Sakuntabhai, A., Ruiz-Perez, V., Carter, S., Jacobsen, N., Burge, S., et al., 1999. Mutations in ATP_2A_2, encoding a Ca^{2+} pump, cause Darier disease. Nat. Genet. 21, 271–277.
Sando, G.N., Howard, E.J., Madison, K.C., 1996. Induction of ceramide glucosyltransferase activity in cultured human keratinocytes. J. Biol. Chem. 271, 22044–22051.
Schaller, G., Meyer-Hermann, M., 2007. A modelling approach towards epidermal homoeostasis control. J. Theor. Biol. 247, 554–573.
Stekel, D., Rashbass, J., Williams, E., 1995. A computer graphic simulation of squamous epithelium. J. Theor. Biol. 175, 283–293.
Sun, T., McMinn, P., Coakley, S., Holcombe, M., Smallwood, R., MacNeil, S., 2007. An integrated systems biology approach to understanding the rules of keratinocyte colony formation. J. R. Soc. Interface 4, 1077–1092.
Tsutsumi, M., Inoue, K., Denda, S., Ikeyama, K., Goto, M., Denda, M., 2009. Mechanical-stimulation-evoked calcium waves in proliferating and differentiated human keratinocytes. Cell Tissue Res. 338, 99–106.
Tsutsumi, M., Denda, S., Inoue, K., Ikeyama, K., Denda, M., 2009. Calcium ion gradients and dynamics in cultured skin slices of rat hindpaw in response to stimulation with ATP. J. Invest. Dermatol. 129, 584–589.
Tsutsumi, M., Goto, M., Denda, M., 2013. Dynamics of intracellular calcium in cultured human keratinocytes after localized cell damage. Exp. Dermatol. 22, 367–369.
Vandenberghe, M., Raphaël, M., Lehen'kyi, V., Gordienko, D., Hastie, R., et al., 2013. ORAI1 calcium channel orchestrates skin homeostasis. Proc. Natl. Acad. Sci. U.S. A. 110, E4839–E4848.
Walker, D., Sun, T., MacNeil, S., Smallwood, R., 2006. Modeling the effect of exogeneous calcium on keratinocyte and HaCat cell proliferation and differentiation using an agent-based computational paradigm. Tissue Eng. 12, 2301–2309.
Wood, L.C., Jackson, S.M., Elias, P.M., Grunfeld, C., Feingold, K.R., 1992. Cutaneous barrier perturbation stimulates cytokine production in the epidermis of mice. J. Clin. Invest. 90, 482–487.